

MAX-PLANCK-INSTITUT FÜR PLASMAPHYSIK
GARCHING BEI MÜNCHEN

**Electron Temperature Fluctuations in
Drift-Resistive Ballooning Turbulence**

A. Zeiler, J.F. Drake, D. Biskamp

IPP 5/69

August 1996

*Die nachstehende Arbeit wurde im Rahmen des Vertrages zwischen dem
Max-Planck-Institut für Plasmaphysik und der Europäischen Atomgemeinschaft über
die Zusammenarbeit auf dem Gebiete der Plasmaphysik durchgeführt.*

Electron Temperature Fluctuations in Drift-Resistive Ballooning Turbulence

A. Zeiler, J. F. Drake*, and D. Biskamp
Max-Planck-Institut für Plasmaphysik,
EURATOM Association, 85748 Garching, Germany

Abstract

Three-dimensional nonlinear simulations of collisional plasma turbulence are presented to model the behavior of the edge region of tokamak discharges. Previous work is extended by including electron temperature fluctuations \tilde{T}_e . The basic paradigm that turbulence and transport are controlled by resistive ballooning modes in low temperature plasma and nonlinearly driven drift wave turbulence in higher temperature regimes persists in the new system. Parallel thermal conduction strongly suppresses the ability of the electron temperature gradient ∇T_e to drive the turbulence and transport everywhere except the very low temperature region edge of the resistive ballooning regime. As a consequence, over most of the resistive ballooning regime only the density gradient drives the turbulence and the temperature fluctuations are convected as a passive scalar. In the drift wave regime only the density gradient acts to drive the nonlinear instability and the temperature fluctuations have a relatively strong stabilizing influence on the resulting turbulence. The stabilizing effect of the temperature fluctuations in the drift wave regime is a consequence of enhanced damping of density and potential fluctuations resulting from local electron heating. Expressions for the anomalous particle and electron thermal transport coefficients, D and χ_e , are presented, which are independent of the electron temperature gradient.

*Institute for Plasma Research, University of Maryland, College Park, Maryland, 20742, USA

1 Introduction

Turbulence and anomalous transport in the cold plasma edge of toroidal confinement devices such as tokamaks and stellarators are usually investigated using models based on two-fluid equations. A particularly simple drift-wave model was established by Hasegawa and Wakatani [1, 2]. It describes density and potential fluctuations in slab geometry with a homogeneous magnetic field. Drift waves in this model, however, are stabilized if magnetic shear is included [3]. Hence the model was extended by including effects of magnetic curvature leading to resistive ballooning instability [4, 5, 6]. The qualitative structure of the turbulence in the drift-resistive ballooning system is largely controlled by a single parameter α which is a measure of the strength of the diamagnetic effects compared with ballooning. For small values of α resistive ballooning dominates and the drift effects are weak. At high values of α where diamagnetic effects are large, resistive ballooning modes are stabilized [5] and it was expected that the strength of the turbulence would be greatly reduced. It was recently shown [6, 7], however, that in the drift wave regime the turbulence remains robust as a result of a nonlinear drive mechanism. The turbulence is sustained even in the absence of linear instability. The curvature plays no role in this regime of nonlinearly sustained turbulence. In the present work we further extend the model to include electron temperature fluctuations as well as the electron temperature gradient as a source of turbulence. The temperature gradient was the dominant drive of turbulence in the two-dimensional sheared slab [8]. Thus, a key goal of this work is to explore the relative roles of ∇T_e and ∇n in driving the turbulence in the drift wave regime. An alternative approach based on similar equations is being followed by Scott [9].

The electron temperature dynamics do not quantitatively alter the basic picture that there exist two characteristic classes of turbulence: resistive ballooning and nonlinearly sustained drift wave turbulence. On a quantitative level, however, our previous results are significantly altered and because of parallel thermal conduction ∇T_e drives the turbulence and transport in a significantly different way than the density gradient. Deeply in the resistive ballooning regime drift effects and parallel electron thermal conduction are relatively unimportant and ∇T_e and ∇n basically add to drive the transport. Thus, transport levels can be calculated from previous work [6] by rescaling the equations to incorporate ∇T_e into the diffusion rate. As the diamagnetic parameter α is increased, parallel electron thermal conduction very quickly significantly alters the dynamics of fluctuations of T_e compared with the fluctuations of n . As a result even before the diamagnetic effects suppress the magnetic curvature drive, the temperature gradient becomes unimportant in driving the turbulence unless $\nabla T_e \gg \nabla n$. In the drift wave regime parallel heat conduction also suppresses the turbulence drive due to the electron temperature gradient, and the anomalous diffusion coefficients D and χ_e are essentially independent of ∇T_e . In this regime, however, the temperature fluctuations do not simply act as a passive scalar. The density and potential fluctuations pump energy into the temperature fluctuations, enhancing the dissipation in the system and thereby suppressing the nonlinearly sustained turbulence. The suppression of turbulence by the dynamics of

T_e in the drift wave regime implies that transport levels will decrease very rapidly with increasing temperature across the ballooning/drift-wave boundary. Since the transition between L and H modes in tokamaks straddles this boundary, L mode falling in the resistive ballooning regime and H mode falling in the drift-wave regime [6], the strong variation of the transport simply as a result of parameter changes at the transition must be included in any complete theory of the formation of the transport barrier.

The paper is organized in the following way: In Section 2 we introduce the set of equations, which is solved by the numerical method discussed in Section 3. In Section 4 we present our simulation results and discuss the impact of ∇T_e and T_e fluctuations on the turbulence and transport. Finally the main results are summarized in Section 5.

2 Equations

The equations on which we base our simulations are an extension of the drift resistive ballooning equations for density and potential fluctuations [4, 6]. Since the equations have been discussed previously [10] in detail, we only briefly review the derivation. The equations for the plasma density n , the potential ϕ and the parallel flow v_{\parallel} are given by

$$\frac{dn}{dt} - 2n\vec{\kappa} \cdot \vec{v}_{\perp}^0 - \nabla \cdot \left(\frac{nc}{\Omega_i B} \frac{d}{dt} \nabla_{\perp} \phi \right) + \nabla_{\parallel} n v_{\parallel} = 0, \quad (1)$$

$$\nabla \cdot \left(\frac{nc}{\Omega_i B} \frac{d}{dt} \nabla_{\perp} \phi \right) - \frac{2c}{eB} \vec{b} \times \vec{\kappa} \cdot \nabla p_e - \nabla_{\parallel} \frac{j_{\parallel}}{e} = 0, \quad (2)$$

$$\frac{dv_{\parallel}}{dt} = -\frac{1}{nm_i} \nabla_{\parallel} p_e, \quad (3)$$

where $p_e = nT_e$, $\vec{v}_{\perp}^0 = -c\nabla\phi \times \vec{b}/B$, $d/dt = \partial/\partial t + \vec{v}_{\perp}^0 \cdot \nabla$ and $\eta j_{\parallel} = -\nabla_{\parallel} \phi + (1/en)\nabla_{\parallel} p_e + (0.71/e)\nabla_{\parallel} T_e$ including the thermal force (factor 0.71) and with η the Spitzer resistivity, $\vec{b} = \vec{B}/B$ the direction of the magnetic field and $\vec{\kappa} = \vec{b} \cdot \nabla \vec{b}$ the field line curvature.

The ions are assumed to be cold and the electron temperature equation will be specified below. The first term in the continuity equation (1) consists of the local density change and the $E \times B$ convection, the second term arises from the divergence of the $E \times B$ velocity caused by the field line curvature, the third term is the divergence of the ion polarization drift and the last term results from parallel ion flows. The vorticity equation (2) is essentially the quasineutrality condition $\nabla \cdot \vec{j} = 0$, where the divergence of \vec{j}_{\perp} arising from the ion polarization and electron diamagnetic drifts (first and second term) is balanced by that of j_{\parallel} . Equation (3) connects the ion parallel velocity to the parallel pressure gradient.

Previously these equations have been studied for constant T_e . Now we include electron temperature fluctuations which follow the Braginskii-equation [11]

$$\frac{3}{2}n\frac{DT_e}{Dt} + \frac{3}{2}n\vec{v}_{de} \cdot \nabla T_e + p_e \nabla \cdot \vec{v}_e - \kappa \nabla_{\parallel}^2 T_e - \frac{5}{2}\frac{c}{e} \nabla \cdot p_e \left(\frac{\vec{b}}{B} \times \nabla T_e \right) - 0.71 \frac{T_e}{e} \nabla_{\parallel} j_{\parallel} = 0$$

with $\vec{v}_e = \vec{v}_{\perp}^0 + \vec{v}_{\parallel,e} + \vec{v}_{de}$ the total electron velocity, $\vec{v}_{de} = -c/(enB) \vec{b} \times \nabla p_e$ and $D/DT = \partial/\partial t + (\vec{v}_{\perp}^0 + \vec{v}_{\parallel,e}) \cdot \nabla$. The fourth and fifth term are the thermal-gradient heat fluxes, and the last term is the frictional heat flux. The continuity equation

$$\frac{Dn}{Dt} + n \nabla \cdot (\vec{v}_{\perp}^0 + \vec{v}_{\parallel,e}) + \nabla \cdot n \vec{v}_{de} = 0$$

is used to eliminate $\nabla \cdot \vec{v}_e$:

$$p_e \nabla \cdot \vec{v}_e = -T_e \frac{Dn}{Dt} - T_e \vec{v}_{de} \cdot \nabla n = -T_e \frac{Dn}{Dt} + n \vec{v}_{de} \cdot \nabla T_e.$$

The fourth term yields

$$\frac{5}{2}\frac{c}{e} \nabla \cdot p_e \left(\frac{\vec{b}}{B} \times \nabla T_e \right) = \frac{5}{2}n \vec{v}_{de} \cdot \nabla T_e + \frac{5}{2}\frac{c}{e} p_e \left(\nabla \times \frac{\vec{b}}{B} \right) \cdot \nabla T_e.$$

Neglecting the nonlinear convection due to the parallel velocity and using $\nabla \times (\vec{b}/B) \cong (2/B) \vec{b} \times \vec{\kappa}$ (assuming $\vec{j} = 0$) leads to the final equation for T_e

$$\frac{3}{2}n \frac{dT_e}{dt} - T_e \frac{dn}{dt} - \kappa \nabla_{\parallel}^2 T_e - 5 \frac{cp_e}{eB} \vec{b} \times \vec{\kappa} \cdot \nabla T_e - 0.71 \frac{T_e}{e} \nabla_{\parallel} j_{\parallel} = 0. \quad (4)$$

(Note the different meaning of κ , denoting the parallel heat conductivity, and $\vec{\kappa}$, denoting the field line curvature.) The complete set of equations consists of Eqs. (1), (2), (3), and (4).

Since the parallel correlation length of the turbulent quantities is much larger than the perpendicular one, we perform our simulations in a flux tube system with field aligned coordinates [12] in which z lies along the local \vec{B} and x, y are transverse to \vec{B} . The transformation to the usual toroidal coordinate system is defined by [6]

$$x = r, \quad y = a [\theta - (\varphi - \varphi_0)/q] - a\varphi_0/q_a, \quad z = R\varphi. \quad (5)$$

In this coordinate system the operators are given by

$$\nabla_{\parallel} = \frac{\partial}{\partial z}, \quad (6)$$

$$\vec{b} \times \vec{\kappa} \cdot \nabla \cong \quad (7)$$

$$-\frac{1}{R} \left\{ [\cos(2\pi z/L_z) + (2\pi \hat{s}(z - z_0)/L_z) \sin(2\pi z/L_z) - \epsilon] \frac{\partial}{\partial y} + \sin(2\pi z/L_z) \frac{\partial}{\partial x} \right\},$$

$$\nabla f \times \vec{e}_\varphi \cdot \nabla = \frac{\partial f}{\partial y} \frac{\partial}{\partial x} - \frac{\partial f}{\partial x} \frac{\partial}{\partial y}, \quad (8)$$

$$\nabla_\perp^2 = \left\{ \frac{\partial}{\partial x} + [2\pi\hat{s}(z - z_0)/L_z] \frac{\partial}{\partial y} \right\}^2 + \frac{\partial^2}{\partial y^2}, \quad (9)$$

where we have used the abbreviations $\hat{s} = (a/q) dq/dr$, $L_z = 2\pi q_a R$, and $z_0 = R\varphi_0$.

The normalization of the equations is described in Refs. [4] and [6], and is based on the ideal ballooning growth rate and a perpendicular scale length which arises from balancing cross field ion dynamics and parallel electron dynamics. The characteristic time and perpendicular space scales are

$$t_0 = \left(\frac{RL_n}{2} \right)^{1/2} \frac{1}{c_s}, \quad (10)$$

$$L_0 = 2\pi q_a \left(\frac{\nu_{ei} R \rho_s}{2\Omega_e} \right)^{1/2} \left(\frac{2R}{L_n} \right)^{1/4} = 2\pi q_a \left(\frac{ne^2 \eta_{\parallel} \rho_s R}{m_e \Omega_e} \right)^{1/2} \left(\frac{2R}{L_n} \right)^{1/4}. \quad (11)$$

Density and temperature are split into a background part $n_0, T_{e,0}$ and the fluctuations \tilde{n}, \tilde{T}_e . For the fluctuating quantities we obtain the scaling

$$\tilde{n} \sim n_0 \frac{L_0}{L_n}, \quad \phi \sim \frac{B}{c} \frac{L_0^2}{t_0}, \quad \tilde{T}_e \sim T_{e,0} \frac{L_0}{L_n}, \quad v_{\parallel} \sim c_s \frac{L_0}{L_n} \quad (12)$$

with $c_s^2 = T_{e,0}/m_i$, $\rho_s = c_s/\Omega_i$ and $L_n = -n/(dn/dx)$. This leads to the dimensionless equations for the normalized fluctuating quantities n, ϕ, T_e , and v_{\parallel} (note that for convenience we denote the normalized quantities without tildes)

$$\frac{d}{dt} \nabla_\perp^2 \phi + \hat{C} p + \frac{\partial^2 h}{\partial z^2} = D_\phi \nabla_\perp^4 \phi, \quad (13)$$

$$\frac{dn}{dt} + \frac{\partial \phi}{\partial y} - \epsilon_n \hat{C} (\phi - \alpha p) + \epsilon_n \alpha \frac{\partial^2 h}{\partial z^2} + \gamma \frac{\partial v_{\parallel}}{\partial z} = D_n \nabla_\perp^2 n, \quad (14)$$

$$\begin{aligned} \frac{dT_e}{dt} + \eta_e \frac{\partial \phi}{\partial y} - \frac{2}{3} \left\{ \epsilon_n \hat{C} (\phi - \alpha p) - \hat{\alpha} \epsilon_n \alpha \frac{\partial^2 h}{\partial z^2} - \gamma \frac{\partial v_{\parallel}}{\partial z} \right\} - \\ - \frac{2}{3} \kappa_{\parallel} \frac{\partial^2 T_e}{\partial z^2} = D_T \nabla_\perp^2 T_e, \end{aligned} \quad (15)$$

$$\frac{dv_{\parallel}}{dt} + \gamma \frac{\partial p}{\partial z} = 0, \quad (16)$$

with

$$\hat{C} = [\cos(2\pi z) + 2\pi\hat{s}(z - z_0) \sin(2\pi z) - \epsilon] \frac{\partial}{\partial y} + \sin(2\pi z) \frac{\partial}{\partial x}, \quad (17)$$

$$\nabla_\perp^2 = \left[\frac{\partial}{\partial x} + 2\pi\hat{s}(z - z_0) \frac{\partial}{\partial y} \right]^2 + \frac{\partial^2}{\partial y^2}, \quad (18)$$

$$\frac{d}{dt} = \frac{\partial}{\partial t} - \nabla_{\perp} \phi \times \vec{e}_z \cdot \nabla_{\perp} = \frac{\partial}{\partial t} - \left(\frac{\partial \phi}{\partial y} \frac{\partial}{\partial x} - \frac{\partial \phi}{\partial x} \frac{\partial}{\partial y} \right) \quad (19)$$

$$h = \phi - \alpha(n + \hat{\alpha}T_e), \quad p = n + T_e, \quad \alpha = \frac{\rho_s c_s t_0}{L_n L_0}, \quad \gamma = \frac{c_s t_0}{L_z}, \quad \epsilon_n = \frac{2L_n}{R}, \quad (20)$$

$$\eta_e = \frac{L_n}{L_{T_e}}, \quad \kappa_{\parallel} = \frac{\kappa}{n_0} \frac{t_0}{L_z^2} = 1.6\alpha^2 \epsilon_n, \quad \hat{s} = \frac{a}{q_a} \frac{\partial q_a}{\partial r}, \quad (21)$$

and the additional viscosities D_{ϕ} , D_n and D_T . L_{T_e} is defined in analogy to L_n . The parallel thermal conduction κ_{\parallel} varies with the effective charge Z_{eff} of the ions and therefore can be somewhat larger than given in Eq. (21). In Eq. (15) we drop the explicit curvature term of Eq. (4), since it is small and of negligible influence according to several runs which we performed with and without this term. Since we find the parallel diffusion of T_e to be the most important new effect introduced by the T_e -dynamics and to facilitate the comparison to our previous results [6], we drop thermal force and frictional heat flux in Eq. (15) in some of our simulations. Therefore we introduce the additional parameter $\hat{\alpha}$. Without thermal force $\hat{\alpha} = 1$, with thermal force $\hat{\alpha} = 1.71$.

The anomalous particle diffusion rate is defined by

$$\langle \tilde{n}v_r \rangle = D \frac{n_0}{L_n} \quad (22)$$

with $\langle \dots \rangle$ denoting an appropriate average over space (perpendicular to \vec{B}) and time. The heat conductivity is obtained by splitting the heat flux into a part caused by density fluctuations and a part due to the temperature gradient

$$\langle \tilde{p}v_r \rangle = n_0 \chi_e \frac{T_{e,0}}{L_{T_e}} + T_{e,0} D \frac{n_0}{L_n}.$$

With

$$\langle \tilde{p}v_r \rangle = T_{e,0} \langle \tilde{n}v_r \rangle + n_0 \langle \tilde{T}_e v_r \rangle,$$

we obtain the definition of χ_e

$$\chi_e = \frac{L_{T_e}}{T_{e,0}} \langle \tilde{T}_e v_r \rangle. \quad (23)$$

In our normalized units Eqs. (22) and (23) yield

$$D = D_0 \Gamma_n, \quad \Gamma_n = -\langle n \frac{\partial \phi}{\partial y} \rangle, \quad (24)$$

$$\chi_e = \frac{D_0}{\eta_e} \Gamma_{T_e}, \quad \Gamma_{T_e} = -\langle T_e \frac{\partial \phi}{\partial y} \rangle, \quad (25)$$

with

$$D_0 = \frac{L_0^2}{t_0} = (2\pi q_a)^2 \rho_e^2 \nu_{ei} \frac{R}{L_n}. \quad (26)$$

Multiplying Eq. (13) by ϕ , Eq. (14) by n , Eq. (15) by T_e and Eq. (16) by v_{\parallel} and integrating over all space yields the energy theorem

$$\begin{aligned} & \frac{1}{2} \frac{d}{dt} \int dV \left\{ \epsilon_n (\nabla_{\perp} \phi)^2 + n^2 + \frac{3}{2} T_e^2 + v_{\parallel}^2 \right\} = \\ & = - \int dV \left\{ \epsilon_n \left(\frac{\partial h}{\partial z} \right)^2 + \kappa_{\parallel} \left(\frac{\partial T_e}{\partial z} \right)^2 + \frac{\partial \phi}{\partial y} \left[n + \frac{3}{2} \eta_e T_e \right] \right\}, \end{aligned} \quad (27)$$

which is used to monitor the accuracy of the time stepping algorithm.

To unravel the relative roles of ∇n and ∇T_e in driving turbulence and transport, it is useful to compare the basic Eqns. (13)-(16) to those studied previously in the constant T_e system. In particular, if the thermal conduction and thermal force ($\hat{\alpha} = 1.0$) are neglected, the T_e and n equations can be combined into a single equation for the electron pressure $p = n + T_e$,

$$\frac{dp}{dt} + (1 + \eta_e) \frac{\partial \phi}{\partial y} - \frac{5}{3} \epsilon_n \hat{C} h + \frac{5}{3} \epsilon_n \alpha \frac{\partial^2 h}{\partial z^2} + \frac{5}{3} \gamma \frac{\partial v_{\parallel}}{\partial z} = D_n \nabla_{\perp}^2 n + D_T \nabla_{\perp}^2 T_e, \quad (28)$$

Equation (28) corresponds to the n -equation in the n/ϕ -system with $T_e = \text{const}$ [6] and may be transformed to it by rescaling the entire set of equations to a normalization based on the pressure scale length $L_p = L_n/(1 + \eta_e)$ rather than the density scale length L_n (except for the factor $5/3$ in front of the usually small parallel compression term). The normalized diffusion rate then becomes

$$D_0 = (2\pi q_a)^2 \rho_e^2 \nu_{ei} \frac{R}{L_p}, \quad (29)$$

and the energy flux $\langle p v_r \rangle$ replaces the particle flux $\langle n v_r \rangle$ in the n/ϕ -system. We find that the thermal force actually influences the system only very weakly so that different roles of ∇T_e and ∇n in driving the turbulence described by Eqns. (13)-(16) arise from the presence of the parallel conduction in the electron temperature equation. The coefficient of the parallel thermal conduction will therefore play a key role in the discussion of the simulation results which follows.

3 Numerical Algorithm

The numerical algorithm which we use for the present simulations is an extension of the pseudo-spectral scheme described in Ref. [6] for the n/ϕ -system. The equations (13-16) are treated in k -space in the poloidal plane and in configuration space along the magnetic field since due to magnetic shear periodic boundary-conditions may not be used in parallel direction. To make optimal use of the numerical resolution the ∇_{\perp}^2 operator [Eq. (18)] should be as isotropic as possible which requires the quantity $z - z_0$ to be close to zero. Hence we split the flux-tube into several boxes in parallel

direction with z_0 defined locally in each box and match the boxes together explicitly as described in more detail in Ref. [6]. The convolutions due to the nonlinearities are evaluated by transforming to configuration space. Perpendicular damping terms are solved exactly by a conversion to exponential factors [6]. In the equations for ϕ , n , and T_e all terms except the ∇_{\parallel}^2 -terms are discretised in time according to a leapfrog scheme. The remaining parallel diffusion terms must be treated implicitly to avoid a severe time step restriction leading to the following set of linear equations:

$$\begin{aligned} -k_{\perp}^2 \phi + \Delta t \nabla_{\parallel}^2 h &= b^{\phi}, \\ n + \Delta t \epsilon_n \alpha \nabla_{\parallel}^2 h &= b^n, \\ T_e + \frac{2}{3} \Delta t (\hat{\alpha} \epsilon_n \alpha \nabla_{\parallel}^2 h - \kappa_{\parallel} \nabla_{\parallel}^2 T_e) &= b^T, \end{aligned}$$

with

$$\nabla_{\parallel}^2 f \equiv \frac{\partial^2 f}{\partial z^2} = \frac{f_{i+1} - 2f_i + f_{i-1}}{\Delta z^2},$$

and i labeling the collocation points along z . Combining these equations leads to a block tridiagonal system for h and T_e :

$$\begin{aligned} -k_{\perp}^2 h + \Delta t \left[1 + \left(1 + \hat{\alpha}^2 \frac{2}{3} \right) k_{\perp}^2 \epsilon_n \alpha^2 \right] \nabla_{\parallel}^2 h - \frac{2}{3} \Delta t k_{\perp}^2 \alpha \hat{\alpha} \kappa_{\parallel} \nabla_{\parallel}^2 T_e &= b^{\phi} + k_{\perp}^2 \alpha (b^n + \hat{\alpha} b^T), \\ T_e + \frac{2}{3} \Delta t (\hat{\alpha} \epsilon_n \alpha \nabla_{\parallel}^2 h - \kappa_{\parallel} \nabla_{\parallel}^2 T_e) &= b^T. \end{aligned}$$

This set of equations for h and T_e is solved by a tridiagonal LU-decomposition for 2×2 matrices. Afterwards n and ϕ are computed straightforward since h is already known. The parallel velocity v is advanced as described in Ref. [6]. In addition to the viscous terms already introduced we use a k^6 -hyperviscosity in the poloidal plane

$$2 \times 10^{-8} \left(\frac{\partial^2}{\partial x^2} + \frac{\partial^2}{\partial y^2} \right)^3$$

for all quantities, an additional hyperviscosity $1 \times 10^{-8} \nabla_{\perp}^6$ for v_{\parallel} , and a small parallel viscosity

$$1.5 \times 10^{-3} \frac{\partial^2}{\partial z^2}$$

for n , ϕ , and v_{\parallel} to damp modes at the edge of the resolved spectrum.

4 Simulation Results

In our previous work [6] we found that the turbulence of the n/ϕ -system with $T_e = \text{const}$ is characterized by two distinct regimes determined by the diamagnetic parameter α . For low α (~ 0.5) the resistive ballooning growth rate is large and the dynamics of drift waves only weakly affect the resulting turbulence and

	$\alpha = 0.42$	$\alpha = 1.26$
Γ_n , torus outside	0.076 ± 0.016	0.021 ± 0.004
Γ_n , torus inside	0.020 ± 0.006	0.011 ± 0.002
Γ_{T_e} , torus outside	0.084 ± 0.016	0.040 ± 0.008
Γ_{T_e} , torus inside	0.040 ± 0.012	0.030 ± 0.006

Table 1: Transport at outside/inside midplane.

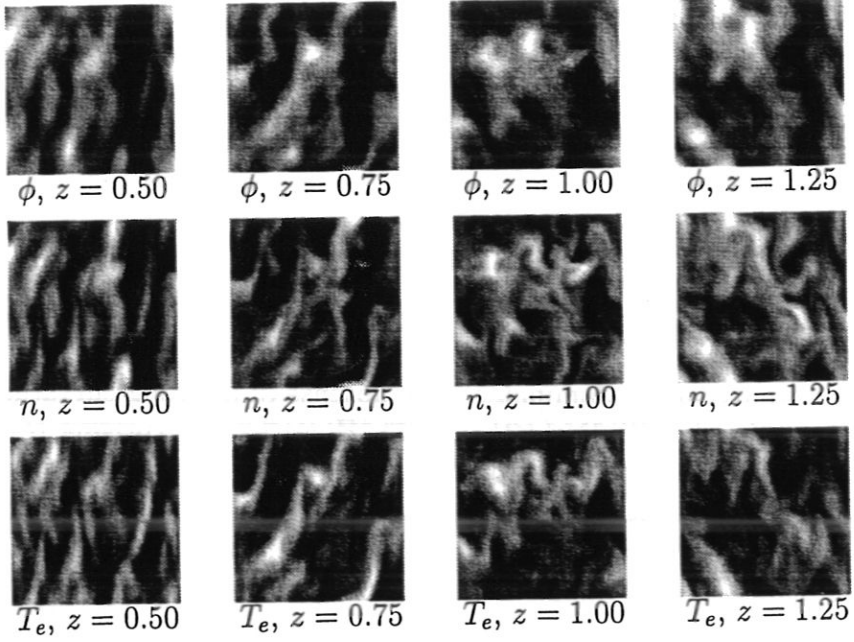
transport. As α increases and approaches 1.5 the curvature plays essentially no role and the drift wave dynamics dominates. The absence of a strong curvature drive in this regime is consistent with linear theory [5]. However, a surprising result is that fluctuations and transport are not strongly reduced in this drift wave regime in spite of the fact that there are no linearly unstable modes [3]. The turbulence is driven by a nonlinear drive rather than a linear drive mechanism [6, 7]. A simple physical model of this nonlinear instability has been presented [7]. We find that the general classification of the turbulence into two regimes is also an accurate description of the more complex system with electron temperature fluctuations. We therefore use the diamagnetic parameter α as a guide in discussing the impact of T_e dynamics on the turbulence.

4.1 Ballooning Regime

We start our discussion of the system including T_e in the ballooning regime where the diamagnetic parameter α is small. The normalized electron parallel thermal conduction κ_{\parallel} is proportional to α^2 as shown in Eqn. (21). Thus, when α is very small, thermal conduction can be neglected and the turbulence and transport are simply driven by the total pressure gradient $\sim 1 + \eta_e$ as discussed at the end of Section 2. The scaling law for transport in this regime is then given by the transport rate in Eqn. (29), with the thermal and particle fluxes linked through η_e , $\Gamma_{T_e} = \eta_e \Gamma_n$. Since the nature of the turbulence in this regime is basically unchanged from the previous system without the electron temperature fluctuations [6], we do not discuss this case further.

Even at relatively small values of α the thermal conduction can no longer be neglected. We present detailed results for $\alpha = 0.42$ with $\epsilon_n = 0.04$, $\eta_e = 1$, $\hat{s} = 1$, $\epsilon = 0.25$, $\gamma = 0.028$, and $\kappa_{\parallel} = 0.07$, including the thermal force $\hat{\alpha} = 1.71$. The resolution was 48×48 complex modes in the perpendicular plane and 96 collocation points along the magnetic field. The box dimensions are $L_x = 6.8$, $L_y = 7.1$, $L_z = 3$, and the viscous damping parameters are $D_{\phi} = D_n = D_T = 4 \times 10^{-3}$. In Fig. 1 we show poloidal cross sections at different locations along \vec{B} (the plots for $\alpha = 1.26$ will be discussed below). We obtain radial streams at the unfavourable curvature location $z = 1$ which break up nonlinearly and form mushroom-like density and

$$\alpha = 0.42$$



$$\alpha = 1.26$$

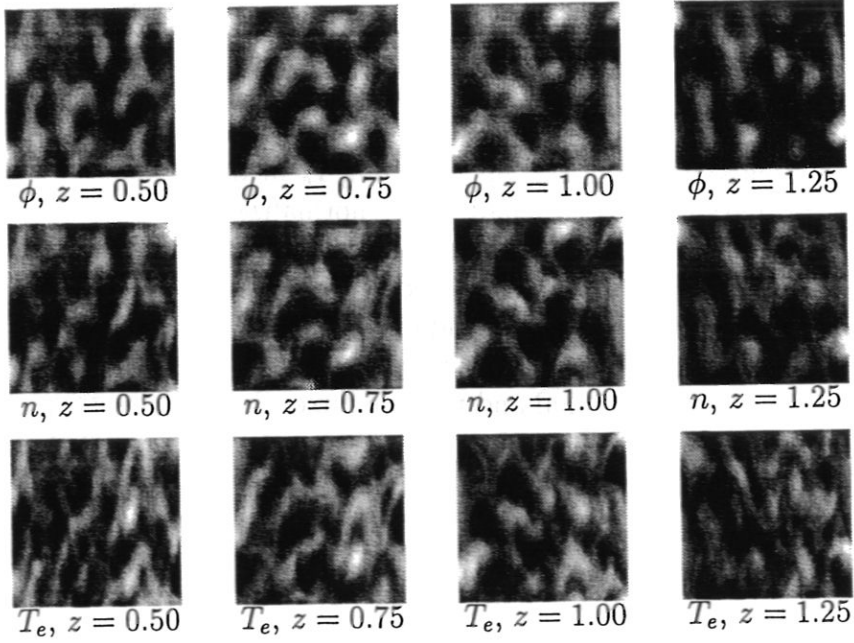


Figure 1: Structure of ϕ , n , and T_e for $\alpha = 0.42$ and $\alpha = 1.26$ at different locations along the magnetic field. The plots show poloidal cross sections at saturation, with $z = 0.5$ corresponding to favourable curvature and $z = 1.0$ to unfavourable curvature. White indicates high and black low values. The poloidal angle increases upwards and density and temperature gradients point to the left.

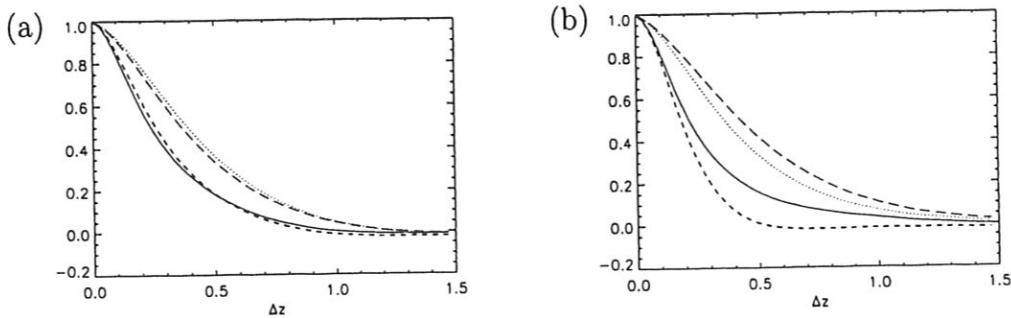


Figure 2: Parallel correlation length for n (solid line), T_e (dotted line), ϕ (dashed line) and h (long dashes); (a) $\alpha = 0.42$, (b) $\alpha = 1.26$

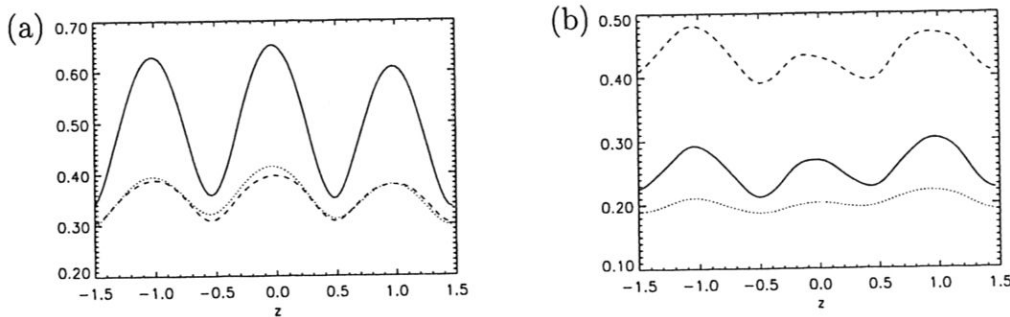


Figure 3: Fluctuation amplitudes of n (solid line), T_e (dotted line), and ϕ (dashed line) as a function of the parallel coordinate; (a) $\alpha = 0.42$, (b) $\alpha = 1.26$

temperature blobs very similar to the case without T_e [6]. Due to the magnetic shear these radial streams become more and more inclined with respect to the radial direction when approaching the favourable curvature region at $z = 0.5/1.5$. This leads to a pattern of intersecting lines on the inside of the torus ($z = 0.5$), which was also reported earlier. Figure 2 shows the parallel correlation lengths of n , ϕ , T_e , and h . The correlation lengths of n and ϕ are the same within the statistical errors. The electron temperature fluctuations are smoothed by parallel heat conduction leading to a significantly longer correlation length.

The average turbulent fluxes are summarized in Table 1. In our normalized units Γ_n and Γ_{T_e} are essentially equal at the outside of the torus. Due to the larger parallel correlation length of T_e the inside/outside asymmetry of Γ_{T_e} is smaller than the asymmetry of Γ_n .

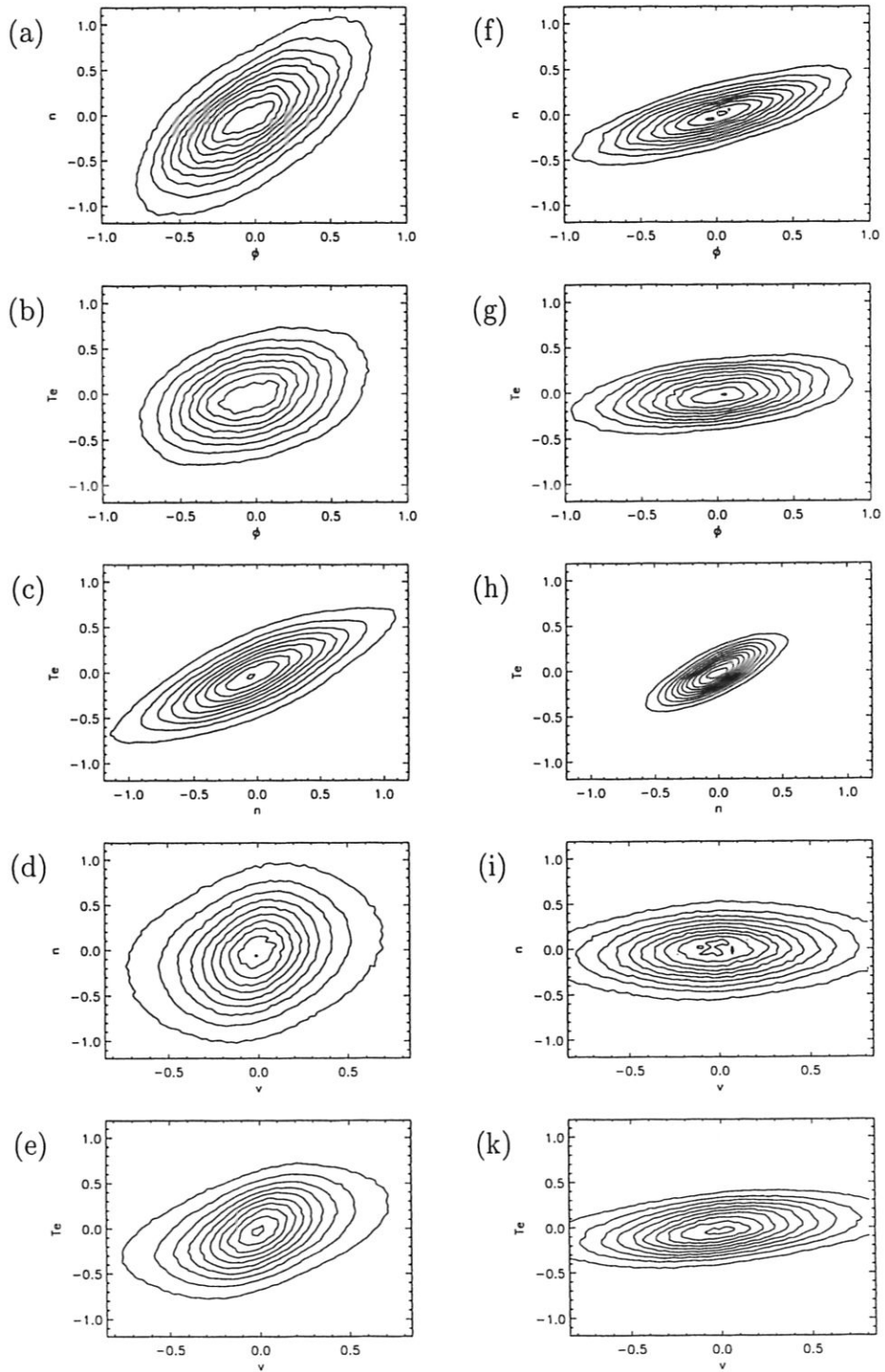


Figure 4: Probability distribution ϕ/n (a,f), ϕ/T_e (b,g), n/T_e (c,h), v_r/n (d,i), and v_r/T_e (e,k) for $\alpha = 0.42$ (a,b,c,d,e) and $\alpha = 1.26$ (f,g,h,i,k)

	$\eta_e = 0.5$	$\eta_e = 1.0$	$\eta_e = 2.0$	without T_e
Γ_n , outside	0.077 ± 0.014	0.076 ± 0.016	0.078 ± 0.018	0.070 ± 0.015
Γ_n , inside	0.023 ± 0.006	0.020 ± 0.006	0.021 ± 0.005	0.035 ± 0.010
Γ_{T_e} , outside	0.038 ± 0.008	0.084 ± 0.016	0.208 ± 0.036	—
Γ_{T_e} , inside	0.019 ± 0.004	0.040 ± 0.012	0.090 ± 0.018	—

Table 2: Transport at outside/inside midplane at different values of η_e .

The time averaged fluctuation amplitudes are shown in Fig. 3. The density fluctuations are more strongly peaked on the outside of the torus than ϕ and T_e fluctuations, reflecting the influence of the parallel heat conduction on T_e . Note that the fluctuation amplitude of n is significantly larger than the one of T_e , despite the fact, that the fluxes are the same $\Gamma_n \cong \Gamma_{T_e}$. A better understanding of this behavior can be gained by looking at the probability distribution functions (Fig. 4). While n and ϕ are more strongly correlated than T_e and ϕ (Fig. 4 a,b), the opposite is true for their correlations with v_r (Fig. 4 d,e), which leads to a larger transport level of T_e for a given fluctuation amplitude. The reason for the relatively strong correlation between T_e and v_r will be discussed further below.

To estimate the relative importance of density and temperature gradients in driving the transport, we vary η_e . Since Γ_n and Γ_{T_e} are of the same magnitude (Table 1) and for $\eta_e = 1$ the drive due to Γ_{T_e} in the energy theorem [Eq. (27)] is larger by a factor 3/2 than the one due to Γ_n , one might argue that temperature gradient and fluctuations provide a more important source of turbulence than the density gradient. We find, however, that, on the contrary, particle and energy diffusion rate react only weakly, if at all, to a change of η_e . The turbulence level is determined by the density gradient and the electron temperature is convected passively without strongly influencing the turbulent $E \times B$ flows.

In Table 2 we summarize particle and heat fluxes from runs with $\eta_e = 0.5/1.0/2.0$ and all other parameters basically as in the run discussed in Section 4.1 (The parameters change slightly, since the computations were carried out in a different normalization). The particle flux is practically independent of η_e and on the outside of the torus is almost the same level as in the system without T_e -dynamics (values taken from Ref. [6]). Note, however, that the inside/outside asymmetry is enhanced in the present system with the T_e -dynamics since the transport on the inside of the torus is considerably reduced. The anomalous heat flux is essentially proportional to η_e . As η_e increases by a factor of four from 0.5 to 2.0, the heat flux Γ_{T_e} increases by a factor of 5.5. The linear relation between the heat flux and η_e results from a corresponding linear relation between T_e and η_e . This can be seen clearly in Fig. 5 where we plot the probability distribution between T_e and v_r for $\eta_e = 0.5/1.0/2.0$. The fluctuation of v_r is essentially unchanged over this range of η_e while T_e increases by essentially a factor of 4.

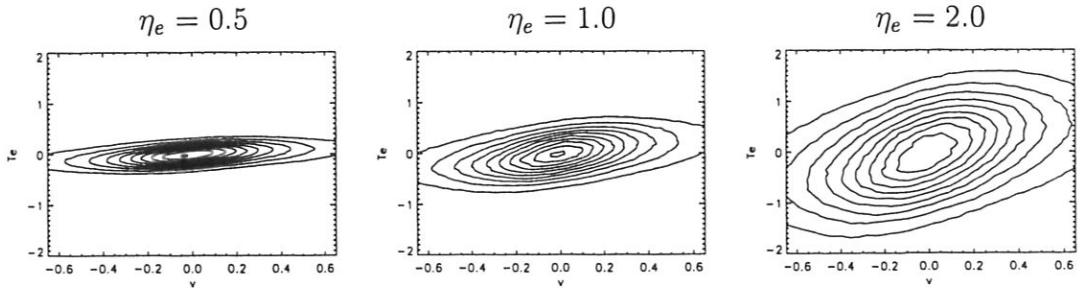


Figure 5: Probability distribution v_r/T_e at different values of η_e

The results in Table 2 and Fig. 5 imply that T_e acts like a passive scalar where the potential and density fluctuations are independent of the dynamics of T_e and the temperature fluctuations result from the convection of the ambient temperature gradient. The insensitivity of n and ϕ to η_e and T_e is a consequence of κ_{\parallel} in the equation for T_e which acts to both reduce the level of thermal fluctuations and the parallel gradient of these fluctuations. To lowest order the T_e equation [Eqn. (15)] reduces to

$$\frac{dT_e}{dt} + \eta_e \frac{\partial \phi}{\partial y} - \frac{2}{3} \kappa_{\parallel} \frac{\partial^2 T_e}{\partial z^2} = D_T \nabla_{\perp}^2 T_e. \quad (30)$$

In this equation the stirring of T_e by the flows is balanced by parallel and perpendicular conduction. Since the equation is linear in the T_e and the drive term $\eta_e \partial \phi / \partial y$ is proportional to η_e , T_e is also proportional to η_e . The relatively strong correlation between T_e and $v_r = \partial \phi / \partial y$ also follows from Eqn. (30). To lowest order, thermal conduction balances the convection across the ambient temperature gradient [$v_r \eta_e$ term in Eqn. (30)] so that $T_e \sim \eta_e v_r$. This effect becomes even more pronounced at higher κ_{\parallel} , and results in a very strong linkage between T_e and v_r .

4.1.1 Transport scaling in the ballooning regime

Ultimately, it is important to deduce from simulations such those presented here a transport coefficient for both particle and energy flux. The difficulty, of course, is that the system of equations describing the turbulence has a substantial number of parameters. Fortunately, consistent with our previous work [6], in the ballooning regime the fluctuations and particle transport are insensitive to parameters such as ϵ_n and the ion sound wave parameter γ . The present simulations demonstrate that because of parallel thermal conduction the diffusion rates of both particles and electron energy are insensitive to ∇T_e if α falls in the range 0.3–0.8. On the other hand, the magnetic shear can significantly impact the level of transport. The particle flux in the ballooning regime typically decreases as the shear parameter \hat{s} deviates from unity [13]. Despite this caveat, we estimate the scaling of the anomalous transport in the common experimentally directly accessible quantities. The normalization of

our system and simulations suggest the following relations for the particle diffusion coefficient D and the heat conductivity χ_e ,

$$D = 0.08 \cdot D_0, \chi_e = 0.09 \cdot D_0 \text{ (torus outside),} \quad (31)$$

$$D = 0.02 \cdot D_0, \chi_e = 0.04 \cdot D_0 \text{ (torus inside),} \quad (32)$$

with the scaling coefficient D_0 defined in Eq. (26). We emphasize that this estimate is based on a small number of numerical simulations in a limited range of the parameter space. It is only valid if κ_{\parallel} is sufficient to suppress the influence of ∇T_e on the turbulence and it does not describe the influence of magnetic shear. These expressions should be regarded only as a first guess, which cannot replace an actual simulation for a given set of experimental parameters.

4.2 Nonlinearly Driven Regime

In the system without electron temperature fluctuations, the resistive ballooning growth-rate is weakened by the diamagnetic effects which become strong when α is large [5]. In this regime the turbulence remains strong and is driven by a nonlinear instability [6, 7]. In this section we show that the electron temperature fluctuations do not alter this result although they substantially weaken the nonlinear instability.

We discuss a run with all parameters as in the reference run of Section 4.1 except $\alpha = 1.26$, $L_x = 9.1$, and $L_y = 9.5$. In the poloidal cross sections (Fig. 1) the radial streams, which are observed in the ballooning dominated regime, disappear and are replaced by almost completely isotropic structures. The particle flux (Table 1) is reduced by a factor of four compared to the ballooning regime and the heat flux by a factor of two. This level of flux is also approximately a factor of four below that calculated earlier in the system without temperature fluctuations. Thus, the fluctuations of T_e have a stabilizing influence on the turbulence in the drift wave regime. Due to the dominant nonlinear drive, which is independent of the curvature, the inside/outside asymmetry is weak. Similarly, we observe little difference in the structure of the turbulence on the inside of the torus compared with that on the outside (see Fig. 1) and the fluctuation amplitudes (Fig. 3) are insensitive to the toroidal location. In contrast to the ballooning regime, where density fluctuations dominate, electron temperature and density fluctuations are of the same magnitude. Since the correlation between T_e and v_r is stronger than the correlation between n and v_r (Fig. 4), as already observed in the ballooning regime, the dimensionless heat flux Γ_{T_e} is larger by a factor of two than the particle flux Γ_n . The parallel correlation lengths of the turbulent quantities are plotted in Fig. 2. The correlation length of ϕ is significantly shorter than in the ballooning regime, while that of h is increased (but is still shorter than the parallel box size).

ϵ_n	η_e	$\hat{\rho}_s^2$	D/\hat{D}_0		χ_e/\hat{D}_0	
			outside	inside	outside	inside
0.02	2.0	0.025	0.059 ± 0.007	0.038 ± 0.008	0.115 ± 0.011	0.087 ± 0.008
0.02	1.0	0.027	0.047 ± 0.006	0.030 ± 0.003	0.081 ± 0.007	0.062 ± 0.006
0.03	0.5	0.045	0.030 ± 0.003	0.016 ± 0.003	0.039 ± 0.004	0.024 ± 0.004
0.04	1.0	0.054	0.015 ± 0.003	0.008 ± 0.002	0.029 ± 0.006	0.022 ± 0.004
0.06	2.0	0.071	0.011 ± 0.002	0.0015 ± 0.0003	0.018 ± 0.003	0.003 ± 0.001
0.06	1.0	0.082	0.006 ± 0.002	0.002 ± 0.001	0.010 ± 0.001	0.006 ± 0.001

Table 3: Transport at $\alpha \simeq 1.25$ and different values of η_e and $\hat{\rho}_s^2$

4.2.1 Effect of η_e , ϵ_n , and κ_{\parallel}

We now want to explore the impact of η_e on the turbulence and transport. To do this it is useful to alter the normalization of the equations to reflect the scaling of the nonlinear drift-wave dynamics rather than that of the resistive ballooning dynamics, which plays no role in this parameter regime. The new transport scaling can be calculated by normalizing the parallel scale length to the magnetic shear length and the time scale to the drift wave time [6, 7, 14]. The transverse length scale then follows from the vorticity equation. The new time and space scales are simply $L_z \sim 1/\hat{s}$, $L_{\perp} \sim \alpha^{1/3}/\hat{s}^{2/3}$, and $t \sim L_{\perp}/\alpha$. The resulting rescaled equations are as follows:

$$\frac{d}{dt} \nabla_{\perp}^2 \phi + \frac{\partial^2 h}{\partial z^2} = D_{\phi} \nabla_{\perp}^4 \phi, \quad (33)$$

$$\frac{dn}{dt} + \frac{\partial \phi}{\partial y} - \hat{\rho}_s^2 \frac{\partial^2 h}{\partial z^2} = D_n \nabla_{\perp}^2 n, \quad (34)$$

$$\frac{dT_e}{dt} + \eta_e \frac{\partial \phi}{\partial y} - \frac{2}{3} \hat{\rho}_s^2 \left(\hat{\alpha} \frac{\partial^2 h}{\partial z^2} + 1.6 \frac{\partial^2 T_e}{\partial z^2} \right) = D_T \nabla_{\perp}^2 T_e, \quad (35)$$

where for simplicity we have not displayed the curvature or parallel flow terms, $h = \phi - n - \hat{\alpha} T_e$, $\hat{\rho}_s^2 = \epsilon_n (\alpha \hat{s})^{4/3}$, and κ_{\parallel} in Eq. (35) has been written in terms of $\hat{\rho}_s$. The anomalous diffusion rate in this drift wave regime is then

$$D = \hat{D}_0 \cdot f(\hat{\rho}_s^2, \eta_e), \quad \hat{D}_0 = D_0 \frac{\alpha^{4/3}}{\hat{s}^{2/3}}. \quad (36)$$

In simulations presented earlier without fluctuations in T_e it was shown that the particle transport is a very strongly decreasing function of $\hat{\rho}_s$ [6, 14]. We explore whether this general trend persists in the presence of T_e fluctuations and whether η_e impacts the fluxes. The transport results normalized to the transport rate \hat{D}_0 are summarized in Table 3. The simulations were carried out for values of α in the vicinity of 1.25 with various values of η_e and ϵ_n at fixed κ_{\parallel} . The variation of

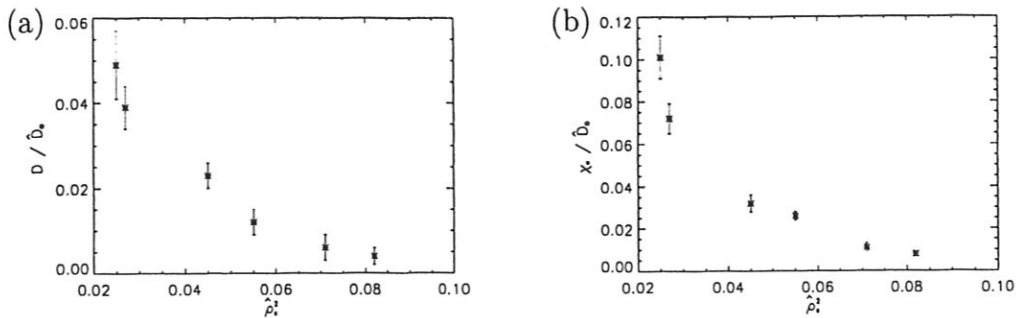


Figure 6: Anomalous particle diffusion coefficient D/\hat{D}_0 (a) and anomalous heat conductivity χ_e/\hat{D}_0 (b) versus $\hat{\rho}_s^2$

ϵ_n and α translates directly into a variation of the normalized variable $\hat{\rho}_s$ as shown in the table. Because both ρ_s and η_e vary in the data of Table 3, it is difficult to separate the influence of these two variables. In Fig. 6 we therefore plot D/\hat{D}_0 and χ_e/\hat{D}_0 versus $\hat{\rho}_s^2$. Since the inside/outside asymmetry is weak, the fluxes in these figures are averaged over the entire simulation domain. Consistent with our previous work [6, 7, 14], we observe a strong drop of the transport with increasing $\hat{\rho}_s^2$. At sufficiently large values of $\hat{\rho}_s^2$, the nonlinear instability is quenched and the residual transport is ballooning driven. Evidence for this result is the re-establishment of the inside/outside asymmetry in flux for large $\hat{\rho}_s^2$ in Table 3.

An important point for understanding the role of η_e is that all of the data for both D and χ_e fall on a single curve. This implies that the transport rates do not depend strongly on η_e , at least for η_e in the range given in Table 3. If they did, Fig. 6 would display significant scatter. The electron temperature gradient is therefore only a weak driver of the turbulence. In a series of simulations at a fixed pressure gradient, the amplitude of the fluctuations decreases with increasing η_e until η_e exceeds 4 and then becomes approximately constant. Thus, for $\eta > 4$ the density gradient ∇n is sufficiently small that the ∇T_e -drive dominates that due to ∇n in spite of the stabilizing influence of κ_{\parallel} .

To understand why η_e drives the turbulence only weakly it is first necessary to discuss the relative roles of $\hat{\rho}_s$ and κ_{\parallel} in damping fluctuations. If all of the drive terms in Eqns. (33)-(35) are neglected, the turbulence will decay as a result of the parallel diffusion until $T_e = h = 0$ and $n = \phi$. Over a longer time scale the sound wave dynamics damp n and ϕ . Thus, the damping of T_e fluctuations is fundamentally a faster process than the damping of n and ϕ . The function h typically damps on the same time scale as T_e . In this simple system the parallel thermal conduction plays the key role in forcing $T_e \rightarrow 0$. In the absence of thermal conduction all three fluctuating quantities can remain nonzero with $h \rightarrow 0$. The inability of ∇T_e to strongly drive the turbulence in comparison to the density gradient is therefore a consequence of

κ_{\parallel}	Γ_n	Γ_{T_e}
0	0.24 ± 0.03	0.180 ± 0.020
0.07	0.017 ± 0.004	0.040 ± 0.008

Table 4: Influence of parallel heat conduction onto the nonlinear drive mechanism. The parameters are the same as in Section 4.2 except for κ_{\parallel} . The curvature terms are switched off ($\hat{C} \equiv 0$) to remove the residual ballooning instability and the thermal force is neglected ($\hat{\alpha} = 1$).

κ_{\parallel} , which strongly suppresses the thermal fluctuations. In contrast, $\hat{\rho}_s$ forces $n \simeq \phi$ but allows both to remain finite so that the nonlinearities of the system can force a phase difference between the two and therefore drive the transport.

The impact of κ_{\parallel} on the transport was investigated in two simulations with identical parameters but with $\kappa_{\parallel} = 0.0/0.07$. The results are presented in Table 4. To remove the residual ballooning drive the curvature terms were discarded. The particle diffusion rate increases by a factor of three to four over the value obtained from the system with $T_e = \text{const}$ as a result of the enhanced drive due to ∇T_e . Thus ∇T_e strongly drives the turbulence in the absence of thermal conduction. Switching κ_{\parallel} to 0.07 reduces Γ_n by a factor 15, leading to a transport level approximately four times below the one obtained for $T_e = \text{const}$. The parallel conduction therefore essentially eliminates the η_e drive of the nonlinear instability. Further increases on the parallel conduction by up a factor of four produce almost no change in the transport rates.

A possible explanation for the reduction of the transport below the level in the system without T_e fluctuations is simply that in the absence of a drive due to η_e the T_e fluctuations act as a sink on the fluctuations of n and ϕ which drive the nonlinear instability. The coupling occurs through the term proportional to h in Eqn. (35). The n and ϕ drive T_e , leading to an energy loss of n and ϕ . This enhanced damping only disappears in the limit $\kappa_{\parallel} \rightarrow \infty$. To make this more explicit we assume that κ_{\parallel} eliminates the η_e drive in Eqn. (35). A crude estimate of the effective dissipation through the temperature equation can then be obtained by writing an equation for $\hat{p} = n + \hat{\alpha}T_e$ by multiplying Eqn. (35) by $\hat{\alpha}$ and adding the result to Eqn. (34). The result is

$$\frac{d\hat{p}}{dt} + \frac{\partial\phi}{\partial y} - \left(1 + \frac{2}{3}\hat{\alpha}^2\right)\hat{\rho}_s^2 \frac{\partial^2 h}{\partial z^2} = \frac{3.2}{3}\hat{\alpha}\hat{\rho}_s^2 \frac{\partial^2 T_e}{\partial z^2} \quad (37)$$

where $h = \phi - \hat{p}$ and for simplicity the perpendicular transport terms have been neglected. If the parallel thermal conduction on the right side of this equation is neglected then this equation coupled with the vorticity equation are identical to the $T_e = \text{const}$ -system but with the $\hat{\rho}_s^2$ parallel damping multiplied by a factor of $1 + 2\hat{\alpha}^2/3$. Because of the rapid decrease of the flux with increasing $\hat{\rho}_s^2$, the increase in the effective value of $\hat{\rho}_s^2$ is sufficient to explain the drop in the transport rate with

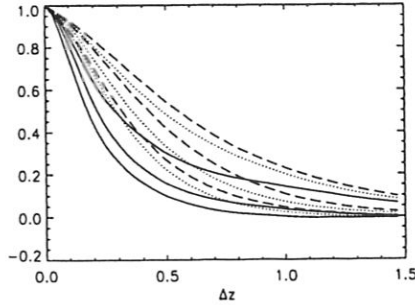


Figure 7: Parallel correlation length for n (solid line), T_e (dotted line), and h (long dashes); $\alpha = 1.26$, $\epsilon_n = 0.02/0.04/0.06$ (the lower line corresponds to the lower ϵ_n -value)

the addition of the T_e dynamics.

Finally, we briefly discuss the essential physics behind the rapid drop in the transport rates with increasing $\hat{\rho}_s^2$. An increase in $\hat{\rho}_s^2$ boosts the parallel dissipation and forces $h = \phi - n \rightarrow 0$ [see the parallel diffusion term in Eqn. (34)] so that the turbulence is more adiabatic and cannot extract energy from the ambient gradients. At the same time the turbulence is forced to longer parallel scale lengths where the drift waves which drive the nonlinear instability become very weak [2, 6, 7, 14]. For the runs with $\epsilon_n = 0.02/0.04/0.06$ and $\eta_e = 1$ discussed in Section 4.2.1 the parallel correlation length is plotted in Fig. 7. The drop of the transport level (Table 3) is accompanied by an increase of the parallel correlation length, which results from the increased parallel diffusion.

4.2.2 Transport Scaling in the Nonlinearly Driven Regime

As previously for the ballooning regime we estimate the scaling of the anomalous transport. Assuming a relation $D/\hat{D}_0 \sim \hat{\rho}_s^\nu$ we obtain

$$\frac{D}{\hat{D}_0} = 3 \cdot 10^{-5} \cdot \hat{\rho}_s^{-4}. \quad (38)$$

This transport rate can be reexpressed in terms of the traditional Gyro-Bohm diffusion rate by noting

$$D_{GB} = \frac{cT_e \rho_s}{eB L_n} = \hat{D}_0 \hat{\rho}_s. \quad (39)$$

In dimensional units

$$\hat{\rho}_s = \frac{\rho_s}{\hat{L}_\perp}, \quad \hat{L}_\perp = \left[\frac{(2\pi L_s)^2 \rho_s^2 \nu_{ei}}{2\Omega_e L_n} \right]^{1/3} \quad (40)$$

where \hat{L}_\perp is the characteristic scale length of the turbulence. The particle diffusion rate then becomes

$$D = 3 \cdot 10^{-5} \cdot D_{GB} \hat{\rho}_s^{-5}. \quad (41)$$

The electron heat conductivity χ_e obeys a similar scaling law. However, we have to renew the cautionary discussion of Section 4.1.1 concerning the range of validity and accuracy of these scaling relations.

5 Conclusions

The inclusion of electron temperature fluctuations \tilde{T}_e does not change the basic paradigm described earlier [6] that the turbulence in the edge of tokamaks is controlled by a diamagnetic parameter α . For small α turbulence is driven by resistive ballooning modes and for large α it is driven by a nonlinear drift wave instability. This diamagnetic parameter is defined as

$$\alpha = \frac{\rho_s c_s t_0}{L_n L_0} \quad (42)$$

where the characteristic time and space scales, t_0 and L_0 , of the turbulence in the resistive ballooning regime are given by

$$t_0 = \left(\frac{R L_n}{2} \right)^{1/2} \frac{1}{c_s}, \quad (43)$$

$$L_0 = 2\pi q_a \left(\frac{\nu_{ei} R \rho_s}{2\Omega_e} \right)^{1/2} \left(\frac{2R}{L_n} \right)^{1/4}. \quad (44)$$

In the present paper we have developed an understanding of the role of the electron temperature gradient ∇T_e and temperature fluctuations \tilde{T}_e in controlling fluctuations and transport. Parallel electron thermal conduction strongly suppresses the effectiveness of ∇T_e in driving the turbulence. Only at the very low temperature edge of the resistive ballooning regime does the ∇T_e drive survive. Elsewhere in the ballooning regime the ∇T_e and T_e fluctuations have essentially no effect. The electron temperature effectively acts like a passive scalar which is convected by the potential fluctuations which are driven by the density gradient. In the high α nonlinear drift wave regime parallel thermal conduction again prevents ∇T_e from driving the turbulence. In this regime, however, the temperature fluctuations do not act as a passive scalar. The dissipation of density and potential fluctuations is enhanced by coupling to the T_e fluctuations. As a consequence, the nonlinear drift wave instability is strongly weakened compared with the system without temperature fluctuations. Anomalous transport coefficients for the density and electron thermal energy, D and χ_e , are presented in both the resistive ballooning and drift wave regimes and are independent of the electron temperature gradient.

References

- [1] A. Hasegawa and M. Wakatani, *Phys. Rev. Lett.* **50**, 682 (1983).
- [2] D. Biskamp, A. Zeiler, *Phys. Rev. Lett.* **74**, 706 (1995).
- [3] P. N. Guzdar, L. Chen, P. K. Kaw, and C. Oberman, *Phys. Rev. Lett.* **40**, 1566 (1978).
- [4] P. N. Guzdar, J. F. Drake, D. C. McCarthy, A. B. Hassam, and C. S. Liu, *Phys. Fluids B* **5**, 3712 (1993).
- [5] S. V. Novakovskii, P. N. Guzdar, J. F. Drake, and C. S. Liu, *Phys. Plasmas* **2**, 781 (1995).
- [6] A. Zeiler, J. F. Drake, D. Biskamp, and P. N. Guzdar, "Three-dimensional fluid simulations of tokamak edge turbulence", *Phys. Plasmas*, in press (1996).
- [7] J. F. Drake, A. Zeiler, and D. Biskamp, *Phys. Rev. Lett.* **75**, 4222 (1995).
- [8] B. D. Scott, *Phys. Rev. Lett.* **65**, 3289 (1990); B. D. Scott, *Phys. Fluids B* **4**, 2468 (1992).
- [9] B. D. Scott, in *Proceedings of the 22nd European Physical Society Conference on Controlled Fusion and Plasma Physics* (European Physical Society, Bournemouth, 1995), Vol. 1, p. 229.
- [10] J. F. Drake, and T. M. Antonsen, *Phys. Fluids* **27**, 898 (1984).
- [11] S. I. Braginskii, "Transport Processes in a Plasma", *Reviews of Plasma Physics*, Vol. 1 (Consultants Bureau, New York, 1965), p. 205
- [12] A. M. Dimits, *Phys. Rev. E* **48**, 4070 (1993); M. A. Beer, S. C. Cowley, and G. W. Hammett, *Phys. Plasmas* **2**, 2687 (1995).
- [13] T. M. Antonsen, J. F. Drake, P. N. Guzdar, A. B. Hassam, C. S. Liu, and S. V. Novakovski, *Phys. Plasmas* **2**, 3712 (1996).
- [14] A. Zeiler, D. Biskamp, and J. F. Drake, "Three-dimensional collisional drift-wave turbulence, role of magnetic shear", *Phys. Plasmas*, in press (1996).